Thermomechanical characterization of leathers under tension using infrared thermography

G. Corvec, N. Di Cesare, X. Balandraud, Jean-Benoit Le Cam, J. Gauffreteau

Thermomechanical characterization of leathers under tension using infrared thermography

Guillaume Corvec[1,2], Noëlie Di Cesare[3], Xavier Balandraud[4,*], Jean-Benoit Le Cam[1,2], and Julien Gauffreteau[5]

[1] CNRS, IPR (Institute de Physique de Rennes), UMR 6251, Univ Rennes, 35000 Rennes, France
[2] Joint Research Laboratory, Cooper Standard - Institut de Physique, UMR 6251, LC-DRIME, Campus de Beaulieu, Bât. 10B, 35042 Rennes Cedex, France
[3] IRDL, UMR CNRS 6027, Université Bretagne Sud, 56321 Lorient, France
[4] CNRS, SIGMA Clermont, Institut Pascal, Université Clermont Auvergne, 63000 Clermont-Ferrand, France
[5] SIGMA Clermont, Campus Design, Matériaux & Innovation, 63170 Aubière Cedex, France

Leather materials are subjected to various deformation states during their elaboration and their use as a final product. Although the mechanical response of leathers under tension has been studied in the literature for decades, scarce information is available on the nature of their elasticity and more generally on their thermomechanical behavior. In the present study, four leathers were tested under uniaxial loading conditions while temperature changes were measured at the specimen surface using infrared thermography. Two types of tests were performed at constant ambient temperature: monotonous displacement-con-trolled tests until failure and cyclic load–unload tests with increasing ampli-tudes. The heat sources at the origin of the temperature changes were also determined by using a version of the heat diffusion equation applicable to homogeneous tests. Results enabled us to discuss the nature of thermoelastic couplings in leathers. Intrinsic dissipation caused by mechanical irreversibility was also detected and quantified. Distinct responses are evidenced depending on the type of leather tested.

Introduction

The mechanical response of stretched leathers has been studied in the literature for decades [1–8]. However, only scarce information is available on the nature of their elasticity and more generally on their thermomechanical behavior. Some physical phenomena involved in their deformation mechanisms have been proposed to model the mechanical response in terms of stiffness, rupture or relaxation. Beyond mechanical tests, some measurements have been taken using infrared (IR) thermography to analyze temperature variations at the surface of leathers. Two approaches are reported in the literature:

Address correspondence to E-mail: xavier.balandraud@sigma-clermont.fr

- non-destructive control of final leather products [9]. Pulsed-phase thermography was performed to evaluate the quality of the leathers in terms of hidden scratches and texture in depth;
- analysis of the thermal response of leathers under mechanical loading, especially self-heating under cyclic loading [10–12], in order to define a limit of acceptable damage for leather products.

The present study belongs to the latter type of approach and aims to study the thermomechanical response of leathers under different types of mechanical loading. The objective is to improve knowledge on the mechanical behavior of leathers via temperature measurements, at the same time enabling us to review their elasticity, viscosity and damage.

Any material produces or absorbs heat when mechanically loaded, due to thermomechanical couplings. The latter are composed of couplings between the temperature and the elastic strain (thermoelastic couplings) and couplings between the temperature and the other state variables. Two types of thermoelastic coupling can be distinguished:

- "classical" thermoelastic coupling, which occurs in metallic materials and polymers below their glass transition temperature; this is sometimes called *isentropic coupling* [13] and leads to a temperature decrease when the material is stretched;
- *entropic coupling*, which mainly occurs in rubber-like materials [14]. It leads to a temperature increase when the material is stretched.

It should be noted that rubbery materials feature both types of thermoelastic coupling: At low stretches ($< 10\%$), the temperature decreases, meaning that the effect of isentropic coupling is greater than that of entropic coupling. At higher stretches, entropic coupling becomes preponderant and the temperature increases [15, 16].

When mechanical irreversibility such as plasticity, fatigue damage and viscosity occurs, heat is produced (the corresponding heat power density is called *intrinsic dissipation* or *mechanical dissipation*) and material self-heating is induced. Measuring temperature changes at the surface of specimens is therefore relevant in order to improve our understanding of the behavior of materials. However, temperature is affected by heat diffusion and heat exchanges with the specimen's environment (through conduction with the jaws of the testing machine, convection with the ambient air, and radiation). This is why, heat sources are generally preferred to temperatures in analyzing material behavior, since they correspond by definition to a quantity which is not affected by heat diffusion and heat exchanges. By "heat source," we mean the heat power density in W/m^3 produced or absorbed by the material itself due to a change in its thermodynamic state. The calculation of heat sources enables, for instance, the quantification of the intrinsic dissipation over a thermodynamic cycle, even under non-adiabatic conditions. In practice, the heat source fields can be reconstructed from the temperature fields using the heat diffusion equation [17, 18]. This equation can be simplified when the heat sources are homogeneous in the specimen, i.e., when the strain fields are homogeneous. In this case, a zero-dimensional (0D) formulation of the heat diffusion equation can be used. This approach has been successfully applied to rubbers [19–25], shape memory alloys [26–32], polyamide 6.6 [33–37], PMMA [38], aluminum alloy [39], steel [40] and copper [38, 41]. To the best of the authors' knowledge, heat source calculations have never been performed for leathers.

In the present study, four leathers were tested under different uniaxial mechanical loadings while temperature changes were measured at the specimen surface using IR thermography. Two types of tests were performed at constant ambient temperature: monotonous displacement-controlled tests until failure and cyclic load–unload tests with different stretch amplitudes.

Experimental setup

Four types of leather, denoted A, B C and D in the following, were tested. Table 1 summarizes the thickness and type of each specimen. Animal hides are usually sliced into several layers: The *grain* leather (also named top-grain leather or top-side leather) is the upper part of the hide, while the *split* leather is the underside. It should be noted that leathers B and D contained a plasticizer. This was highlighted by spectrophotometric analysis, which revealed the presence of an ester group COOR. The presence of plasticizer in leathers B and D was confirmed by thermogravimetric analysis (TGA). It is to be noted

Table 1 Characteristics of the four tested leathers. The time constant τ in the final column characterizes the ability of the specimen to exchange heat with the external environment; see Eq. (1) in "Data processing for heat source calculation" section

Designation	Animal	Type	Thickness (mm)	Remark	Time constant τ (s)
A	Cow	Split	3.1		90
B	Calf	Split	2.3	Presence of plasticizer	53
C	Pig	Grain	1.0		80
D	Calf	Grain	1.8	Presence of plasticizer	57

that leather D was mechanically softened (operation consisting of pummeling the leather with a pin wheel) during the elaboration process and fed by a fatty acid during re-tanning.

The experimental setup is presented in Fig. 1. Rectangular specimens (5 mm in width and 110 mm in length) of each leather type were cut from a sheet; see Fig. 1a. These dimensions differed from the recommendations of ASTM standards D2209 and D2211

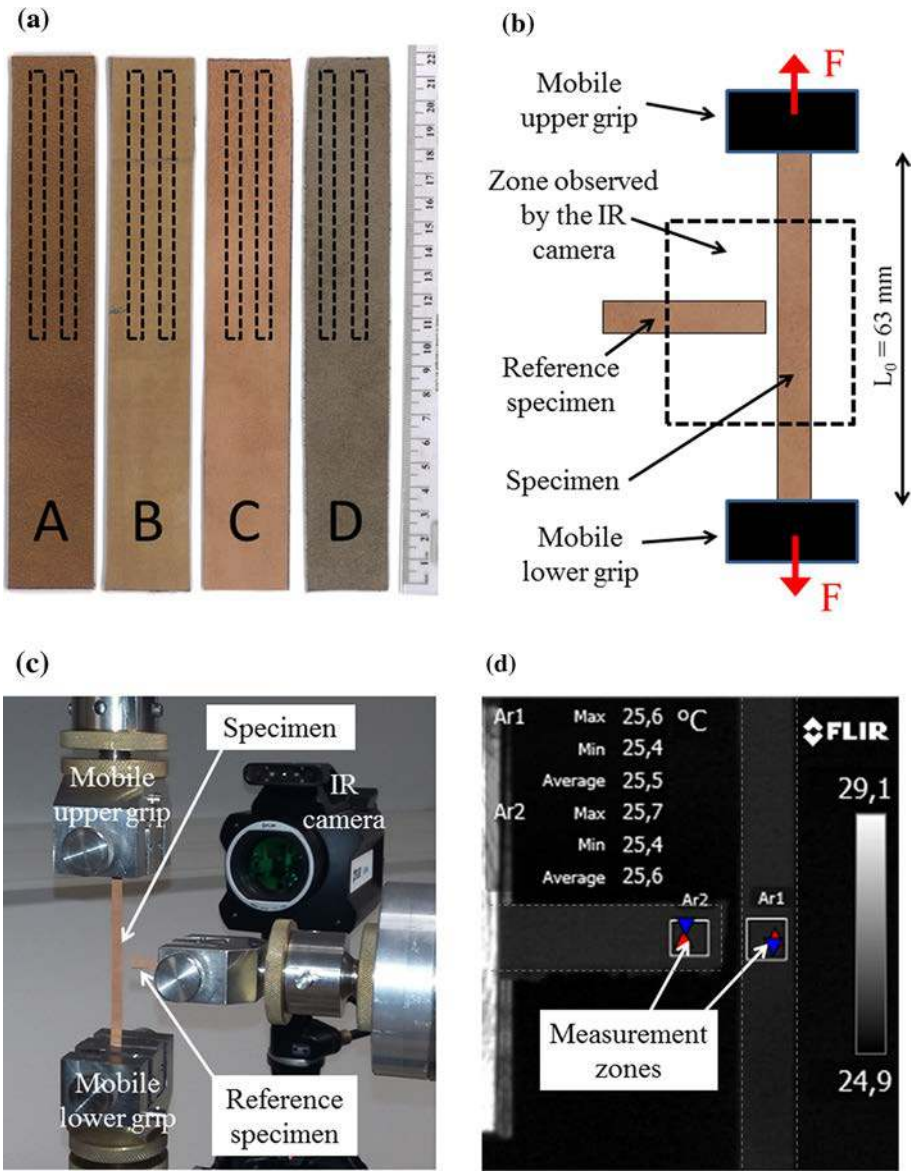

Figure 1 Experimental setup: **a** four leather sheets used to extract specimens for uniaxial tensile tests, **b** schematic view of the measurement zone featuring the tested specimen and a reference specimen, **c** photograph of the experiment, **d** location of the two temperature measurement zones during each test.

[42, 43] dedicated to the measurement of the elongation and strength in tension of leather, but it should be recalled that the objective of the present study is to improve knowledge of the thermomechanical behavior of leathers via temperature measurements using an IR camera. Dimensions were thus chosen as a compromise between machine capability and the ability to detect temperature change due to stretching. Uniaxial tests were performed using a homemade biaxial testing machine featuring four independent IAI electrical actuators (RCP4-RA6C-I-56P-4-300-P3-M) driven by a PCON-CA 56P I PLP 2 0 controller, four PCON-CA (IAI) controllers coupled to an in-house LabView program, and four load cells with a capacity of 1094 N. In the present study, the testing machine was used to stretch the specimens with the two vertical actuators (initial distance L_0 between the grips set to 63 mm, corresponding to the specimens' useful length), while one horizontal actuator was used to move a *reference specimen* close to the tested one: see Fig. 1b. The role of the reference specimen, made of the same leather as the tested one, was to track the temperature variation of the close environment. Reference specimens were therefore not stretched during the tests: see Fig. 1c.

Temperature measurements were taken with a FLIR infrared camera equipped with a focal plane array of 640 × 512 detectors operating in wavelengths between 1.5 and 5.1 μm. The thermal resolution (or noise equivalent temperature difference) was equal to 0.02 °C for temperatures between 5 and 40 °C. The IR camera was powered up 3 h before starting the tests in order to ensure a stable internal temperature. The integration time and the acquisition frequency were set to 1000 μs and 25 Hz, respectively. Calibration of the camera detectors was performed with a black body using a non-uniformity correction (NUC) procedure. The variation in *mean temperature change* of the tested specimen was defined with respect to the reference specimen. It can be noted that spatial averaging operations over the measurement zones (on the tested specimen and the reference specimen, see Fig. 1d) strongly improve thermal measurement resolution. The latter can be estimated to within a few hundredths of a degree.

Analysis of monotonous displacement-controlled tests

A typical nominal stress–stretch curve of each type of leather at 100 mm/min until failure is presented in Fig. 2a. The *nominal stress* is defined as the ratio between the force and the initial area of the specimen's cross section. The *stretch* λ is defined as the ratio between the current length L and the initial length L_0. The value chosen here for the displacement rate differed from the recommendation of ASTM standards D2209 and D2211 (254 ± 50 mm/min) [42, 43]. It also differed from ASTM standard D412 (500 ± 50 mm/min) for vulcanized rubber and thermoplastic elastomers in tension [44]. However, as discussed concerning the choice of specimen dimensions, the objective here to detect temperature change in order to perform a thermomechanical analysis. It

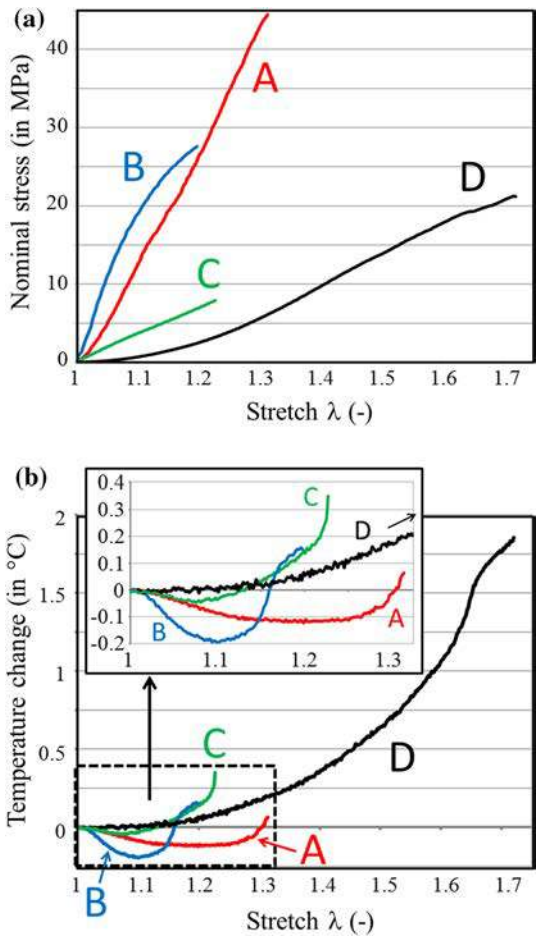

Figure 2 Tensile tests at 100 mm/min until specimen failure: **a** nominal stress with respect to the stretch, **b** temperature change with respect to the stretch.

can be observed in Fig. 2a that split leathers (A and B) are stiffer than grain leathers (C and D). The higher ductility of leather D compared to leather C can be explained by the presence of plasticizer and the softening operation which was performed during the manufacturing process (see Table 1). The nominal stress–stretch curves of leathers A and C are linear, while they are strongly nonlinear for leathers B and D. This can be related to the presence of plasticizer in leathers B and D. Temperature changes with respect to the stretch provide additional information (see Fig. 2b). The following comments can be drawn from these curves:

- split leathers A and B clearly exhibit a strong temperature decrease during the first part of the test ($-$ 0.12 °C at $\lambda = 1.1$ for leather A, $-$ 0.19 °C at $\lambda = 1.2$ for leather B). This response is a clear expression of classic isentropic coupling; see "Introduction" section. Then, the temperature increases and becomes slightly higher than the ambient temperature ($+$ 0.06 °C at failure for leather A, $+$ 0.15 °C at failure for leather B);
- grain leather C also first exhibits a slight temperature decrease ($-$ 0.04 °C at $\lambda = 1.07$), before a significant temperature increase (0.35 °C above the ambient temperature at the end of the test). Note that the slight initial temperature decrease was not clearly observed in other tests performed on leather C (temperature changes of around $-$ 0.01 °C);
- grain leather D is characterized by a nearly isothermal response up to $\lambda = 1.1$, which can be explained by an equilibrium between the effects of isentropic coupling (negative heat "sources") and entropic coupling (positive heat sources) at low stretches. Then, the temperature strongly increases, reaching more than 1.8 °C above ambient at the end of the test. This high temperature increase could be due to entropic coupling and mechanical irreversibility (viscosity and/or damage);
- for the four leathers, global self-heating can be explained by the effects of entropic coupling and/or mechanical irreversibility occurring in the materials. Both effects are associated with the production of a (positive) heat source. The next section goes further into the analysis of the thermomechanical response of the tested materials by considering another type of mechanical loading.

Analysis of cyclic load–unload tests with different stretch amplitudes

This section, dedicated to cyclic tests, is divided into three parts. First, the loading conditions and mechanical responses are presented. Then, the data processing for the heat source calculation from temperature measurements is described. Finally, material behavior is analyzed in terms of temperature change and heat source variation.

Loading conditions and mechanical responses

Loading consisted of four series of 5 load–unload cycles. The series are denoted #1, #2, #3 and #4 (see Fig. 3a), corresponding, respectively, to stretch amplitudes of 25, 50, 75 and 100% of 0.9 λ_{max}, where λ_{max} is the stretch at failure under tension of the considered leather. Two displacement rates were tested: $\pm$ 100 mm/min and $\pm$ 300 mm/min. The factor of three between the two loading rates is a compromise between machine capability and sufficient heat production to distinguish thermoelastic and viscous effects at different stretching rates. For instance, Fig. 3a shows a typical nominal stress–stretch curve obtained for leather B at $\pm$ 100 mm/min. Figure 3b shows the variation in nominal stress as a function of time. Within each series of load–unload cycles, a classic accommodation effect is visible: The maximum nominal stress σ^i_{max} decreases at each cycle (i from 1 to 5). It can be also observed in Fig. 3a that during the first loading stage (i = 1) of each series, the nominal stress recovers the values that would have been attained if the loading had been monotonous. In fact, the nominal stress increases more when the stretch exceeds the previously encountered maximum stretch. These phenomena show a strong similarity with the Mullins effect [45] in rubber (stress softening and stiffness recovery for stretches never applied before). The same trends were obtained for the other three leathers and for the two displacement rates: Fig. 4 shows the values of the ratio $\sigma^i_{max}/\sigma^1_{max}$ within each series of load–unload cycles at $\pm$ 100 mm/min (Fig. 4a) and at $\pm$ 300 mm/min

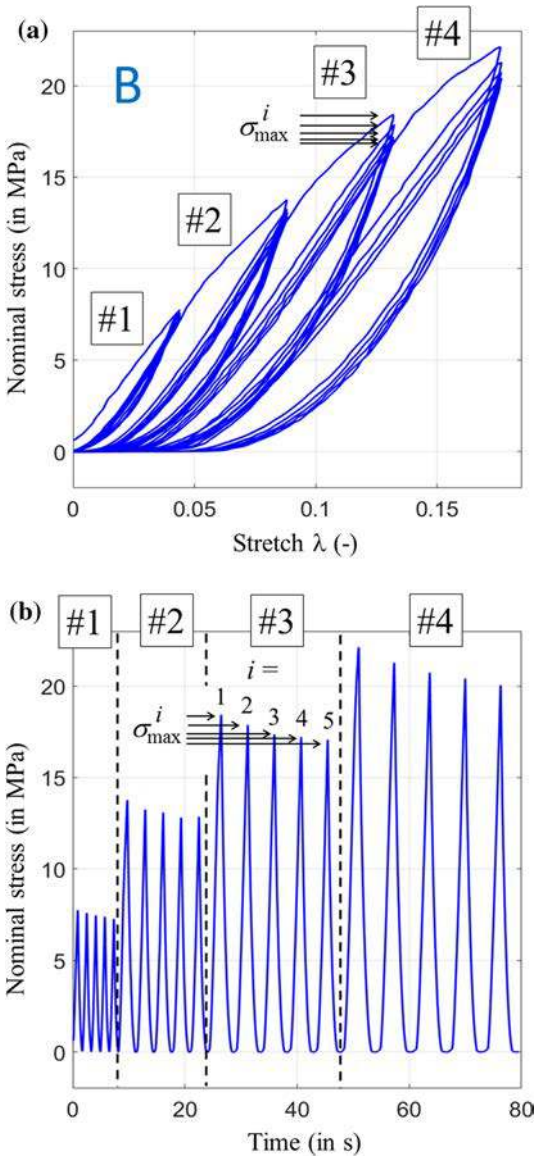

Figure 3 Cyclic test for material B at ± 100 mm/min: **a** nominal stress with respect to stretch, **b** nominal stress with respect to time.

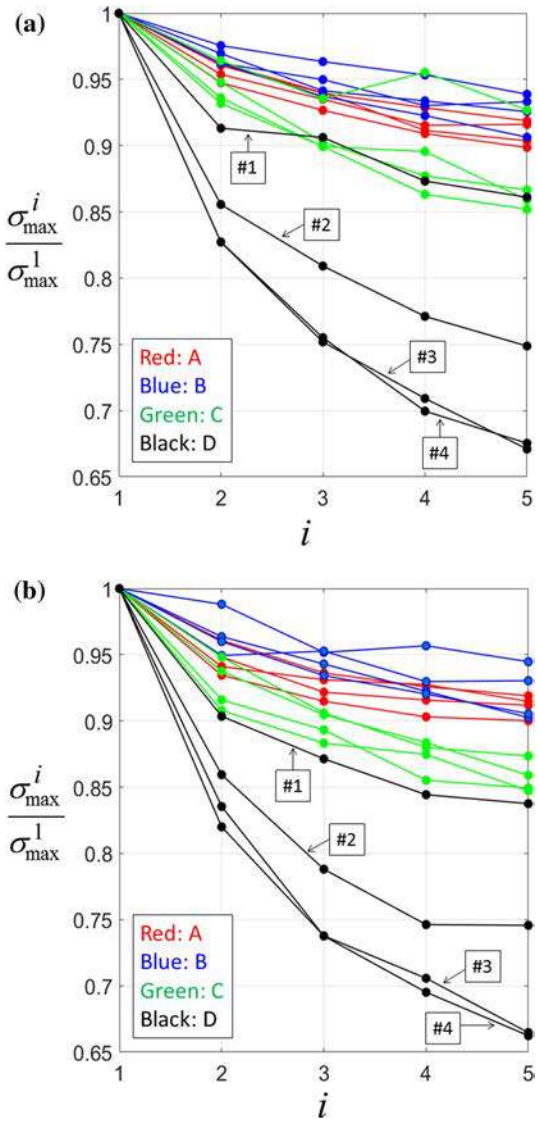

Figure 4 Cyclic tests: ratio of the maximum stress in each load–unload cycle over the maximum stress of the first cycle. The four series of load–unload cycles are denoted #1, #2, #3 and #4 (see Fig. 3a). The cycle number in each series is denoted i. **a** Cycles at ± 100 mm/min. **b** Cycles at ± 300 mm/min.

(Fig. 4b) for all the tested leathers. The following observations can be made with respect to this figure:

- The curves at ± 100 mm/min and ± 300 mm/min are quite similar. This shows that the loading rate has very little impact on the stress softening phenomenon. A similar conclusion was arrived at in Ref. [4] concerning the effect of the loading rate on stress–stain curves;
- The stress softening phenomenon is much greater for grain leathers (C and D) than for split leathers (A and B). At the fifth cycle ($i = 5$), the stress loss is equal to 15% for leather C and 34% for leather D compared to the stress at the first cycle. It is equal to only 10% for leathers A and B;
- For split leathers, the maximum stresses are nearly stabilized at the fifth cycle, especially at ± 300 mm/min (ratios $\sigma_{max}^{i}/\sigma_{max}^{1}$ for $i = 4$ and for $i = 5$ are nearly equal).

As for the monotonous tests in the previous section, additional information can be revealed by analyzing the thermal data.

Data processing for heat source calculation

As mentioned above in "Introduction" section, a zero-dimensional (0D) version of the heat diffusion equation can be used when heat sources are homogeneous in the specimen; That is, when the strain fields are homogeneous (which is the case for the present experiments). This equation can be used to calculate the heat sources produced or absorbed by the material from the knowledge of the mean temperature changes. Equation (1) shows the relation between the heat source s (in W/m^3) and the mean temperature change θ:

$$s = \rho C\left(\frac{d\theta}{dt} + \frac{\theta}{\tau}\right) \tag{1}$$

where ρ is the material density, C the specific heat and τ a time constant characterizing the global heat exchanges with the environment of the specimen. The value of τ was initially measured for each specimen by considering a natural return to ambient temperature, the specimen being placed in the jaws of the testing machine as for the mechanical tests. Indeed, the solution to Eq. (1) for $s = 0$ is an exponential function whose decay constant is τ, which can be easily identified from the experimental temperature decrease. Table 1 provides the values for the four leather specimens.

By dividing Eq. (1) by ρC, we obtain

$$s' = \frac{\mathrm{d}\theta}{\mathrm{d}t} + \frac{\theta}{\tau} \tag{2}$$

where

$$s' = \frac{s}{\rho C} \tag{3}$$

which can still be named "heat source," but then expressed in °C/s. It corresponds to the temperature rate that would be obtained in adiabatic conditions. Note that by using this unit, it is not necessary to know the values for the density and the specific heat. In practice, the heat sources from Eq. (2) can be calculated by finite differences.

Thermal and calorific analysis of the cyclic tests

After some preliminary tests on various samples, cyclic loadings were applied to each type of leather at the two loading rates. It can be noted that, as is usual for full-field measurement techniques, a huge amount of data was recorded (temperature video files of between 50 Mo and 500 Mo per test, depending on the test duration). Figure 5 shows the temperature change and heat source variations for split leather A at the two displacement rates. Time periods corresponding to buckling are highlighted by gray-shaded rectangles in the graphs. The times corresponding to maximum stretching are indicated by vertical solid lines. The following observations can be made concerning this figure:

- a global temperature increase is observed for both displacement rates. The global temperature rate is of about 1.2 mK/s for the test at ± 100 mm/min (global increase of 0.17 °C in 140 s) and about 6.2 mK/s for the test at ± 300 mm/min (global increase of 0.3 °C in 48 s). These global temperature increases can be attributed to viscosity and/or damage. Within each load–unload cycle, the temperature decreases and increases in agreement with an isentropic coupling effect. Results show that temperature fluctuations increased with the stretch rate. However, it is difficult to draw further conclusions because temperature change depends on the heat exchanged with the outside environment of the specimen;
- the heat sources (expressed in °C/s) are negative during loading and positive during unloading. The curves are not piecewise constant, meaning that the heat sources are not only of isentropic coupling type. Indeed, heat sources due to isentropic coupling are proportional to the stretch rate. It was verified that the temporal integration of the heat sources over the whole test duration (total heat produced) is positive, in agreement with the global temperature increase over the duration of the test. This reveals the production of intrinsic dissipation due to viscosity and/or damage. It is interesting to note that during the first loading phase within each series of load–unload cycles (see blue arrows in the graphs), the heat source starts to increase before reaching the maximum stretch. This calorific response confirms the production of intrinsic dissipation, which counters the effect of isentropic coupling.

The same qualitative analysis can be made for split leather B (see Fig. 6) and grain leather C (see Fig. 7), although quantitative differences can be highlighted. For split leather B, the global temperature rate is of about 4 mK/s for the test at ± 100 mm/min and

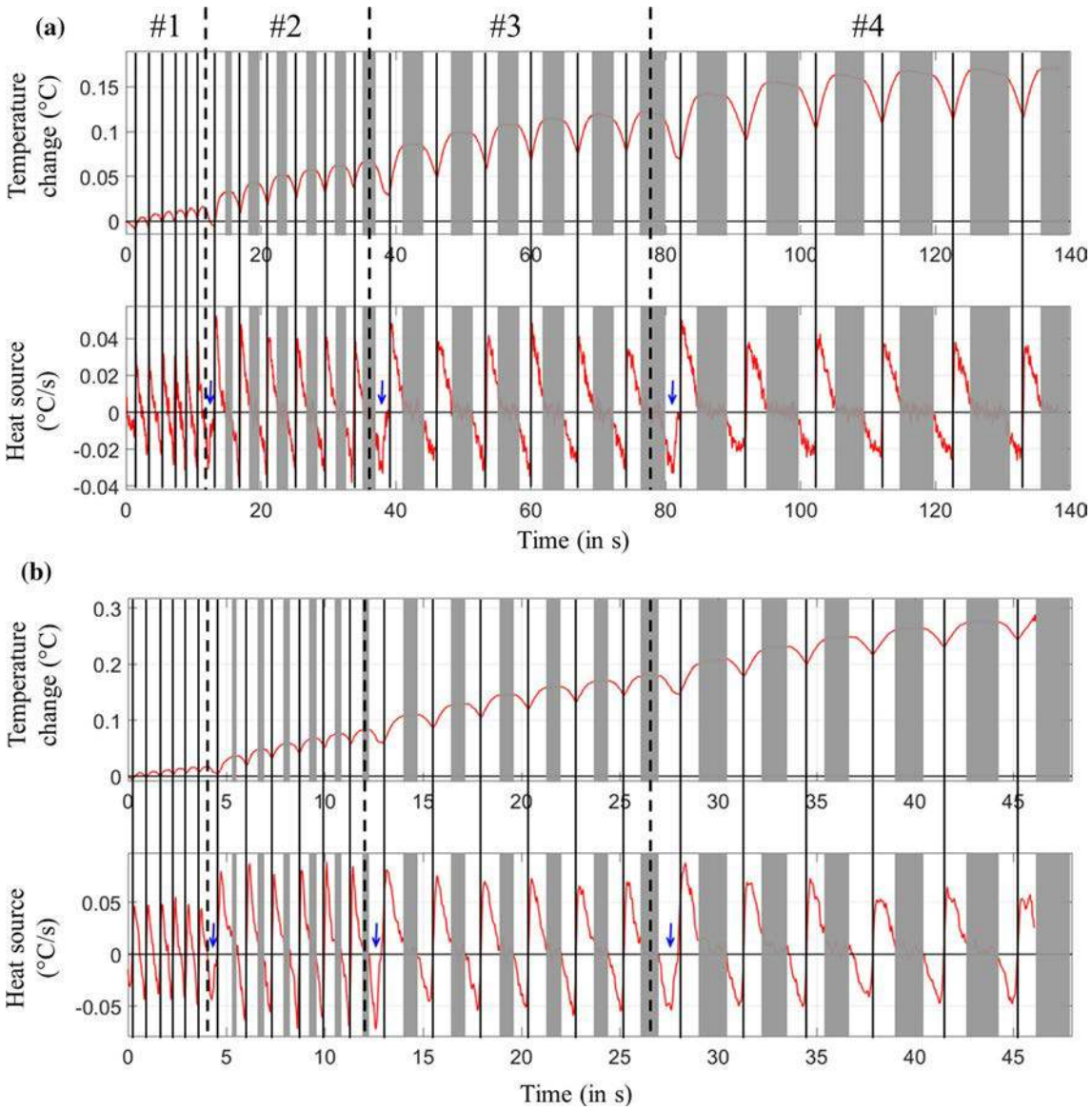

Figure 5 Cyclic tests for leather A. Gray zones correspond to specimen buckling. Vertical black lines correspond to the maximum stretch in each mechanical cycle. **a** Cyclic test at ± 100 mm/min. **b** Cyclic test at ± 300 mm/min.

about 14 mK/s for the test at ± 300 mm/min. These rates are higher than those obtained for the other split leather (A), revealing a greater viscosity effect. This is confirmed by the variations in the heat sources. The heat source starts to increase before reaching the maximum stretch for more loading phases than for leather A: see red arrows in the graph. As a general comment, it can be claimed that the effect of viscosity is calorically much greater in leather B than in leather A, due probably to the presence of plasticizer in the former. For grain leather C (see Fig. 7), the overall trend in terms of temperature increase is less linear. A global temperature rate of about 16 mK/s can, however, be estimated for the test at ± 300 mm/min.

Figure 8 shows the temperature change and heat source variations for grain leather D at the two displacement rates. Graphs are limited to the first three series because the strong buckling in series #4 prevented us from extracting accurate thermal data. The following comments can be made for this figure:

- each loading phase is associated with a temperature increase. This can be attributed to the effect of viscosity and/or entropic coupling. It can be noted that the first loading phase in each series is

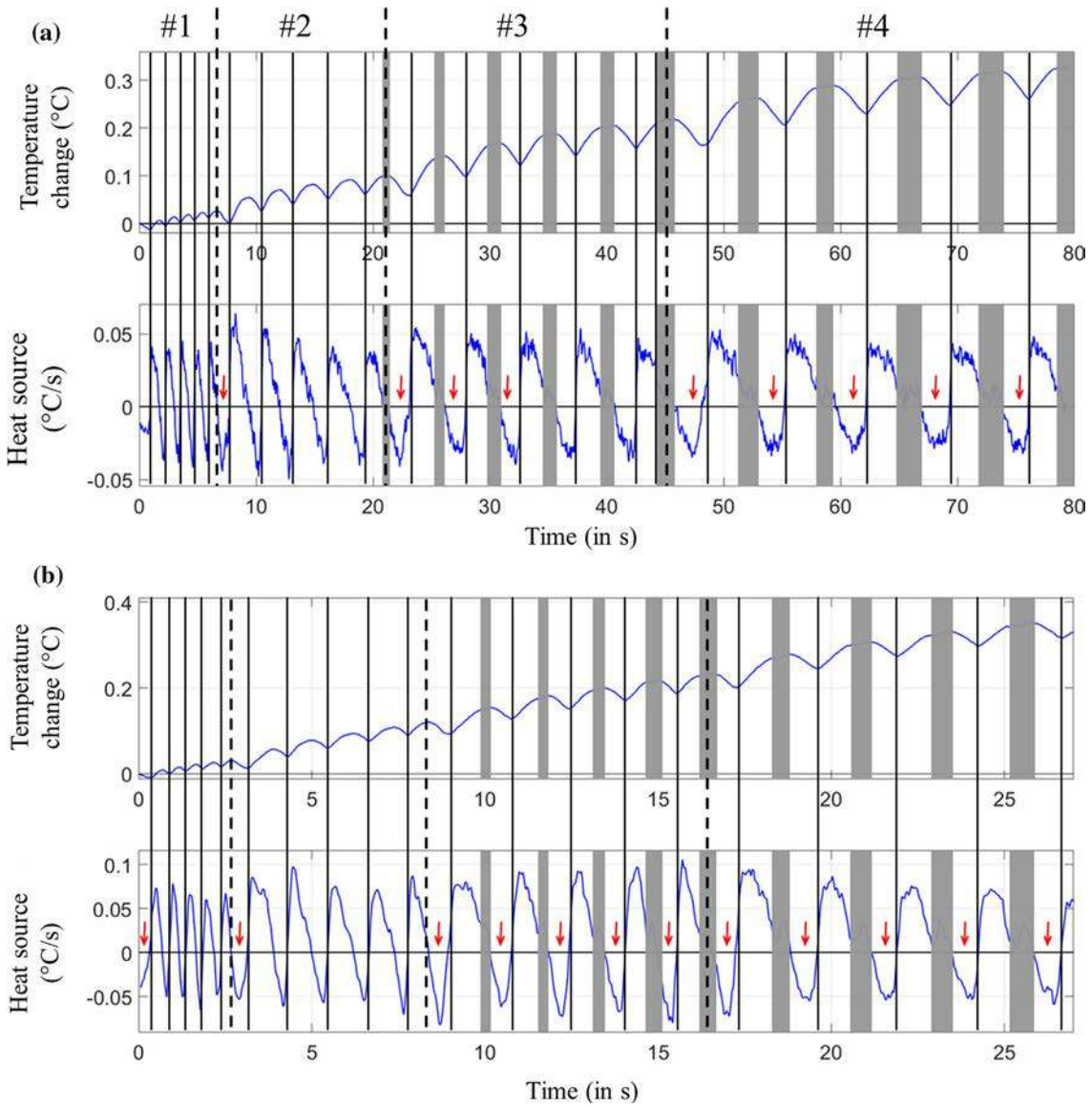

Figure 6 Cyclic tests for leather B. Zones in gray correspond to specimen buckling. Vertical black lines correspond to the maximum stretch in each mechanical cycle. **a** Cyclic test at ± 100 mm/min. **b** Cyclic test at ± 300 mm/min.

associated with a stronger temperature increase than those of the subsequent cycles: see red arrows. This thermal phenomenon can be related to the fact that the stretch exceeds the previously encountered maximum stretch. A similar calorific response was observed to that of the Mullins effect in rubber (see calorific analysis in [21]). Each unloading phase is associated with a temperature decrease. After each strong temperature increase (indicated by the red arrows), the temperature globally decreases, meaning that the calorific effect of viscosity decreases over the cycles;

- the total heat produced by the material over the whole test duration (temporal integration of the heat sources) is clearly positive, showing the strong influence of the viscosity. It can be noted that during the unloading phases, the heat sources are slightly negative, meaning that the viscosity nearly counteracts the entropic effect in terms of heat production.

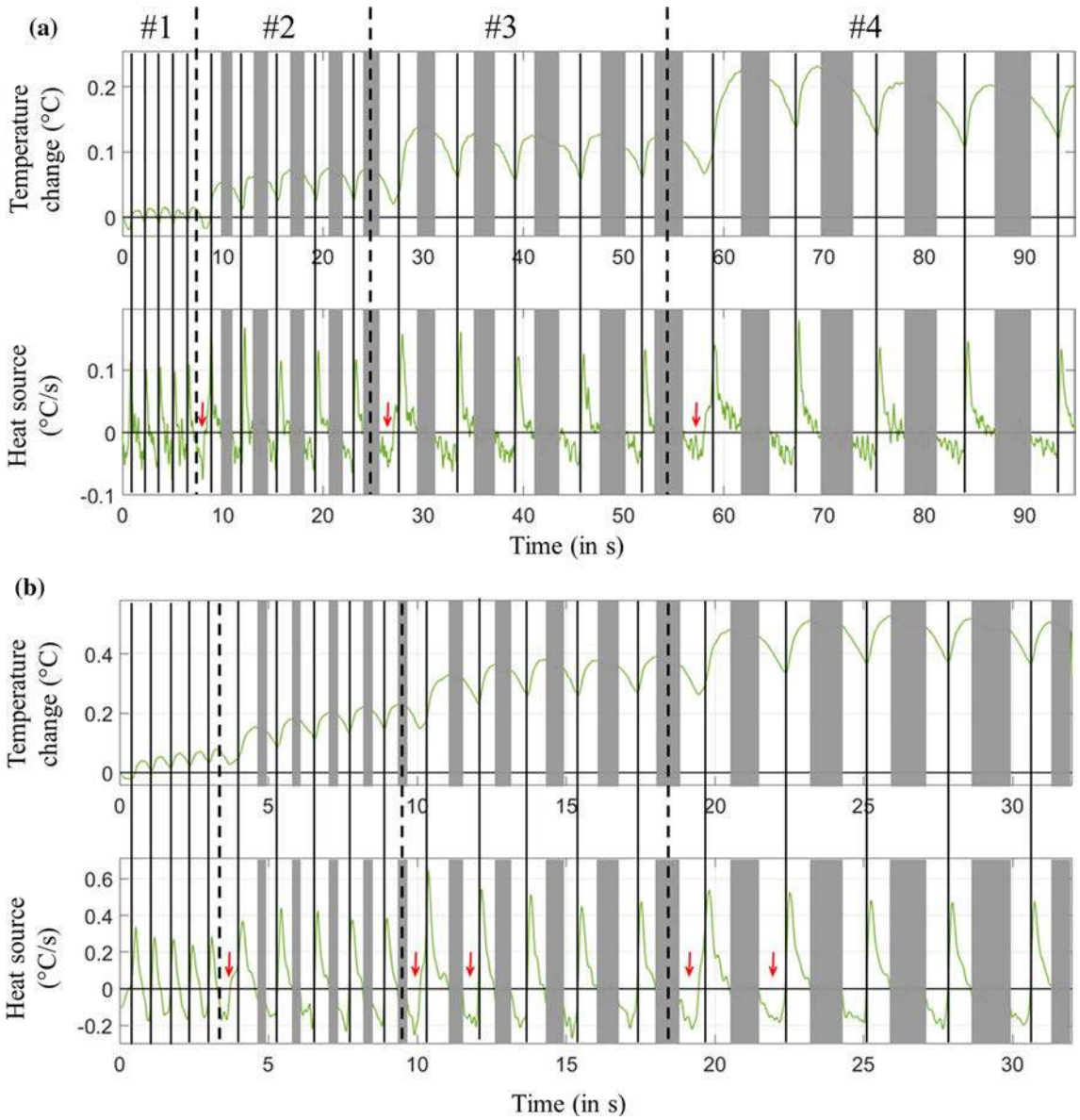

Figure 7 Cyclic tests for leather C. Zones in gray correspond to specimen buckling. Vertical black lines correspond to the maximum stretch in each mechanical cycle. **a** Cyclic test at ± 100 mm/min. **b** Cyclic test at ± 300 mm/min.

Conclusions

The mechanical response under tension of leathers has been studied in the scientific literature for decades. The present study aimed at providing new data concerning their thermomechanical response, namely the temperature changes caused by material stretching. For this purpose, IR thermography and heat source calculations were performed to analyze the response under tension of different leathers. Split leathers and grain leathers were compared during monotonous tests and cyclic tests. Beyond the mechanical responses, the following conclusions can be drawn from the calorific response of the tested specimens:

- the two tested split leathers (cow and calf), as well as the grain pigskin leather, featured "classic" isentropic thermoelastic coupling. Typically, the materials absorbed heat when starting the loading under tension;
- the tested grain calf leather, which was mechanically softened during the elaboration process and fed by a fatty acid during re-tanning, featured entropic thermoelastic coupling, such as in

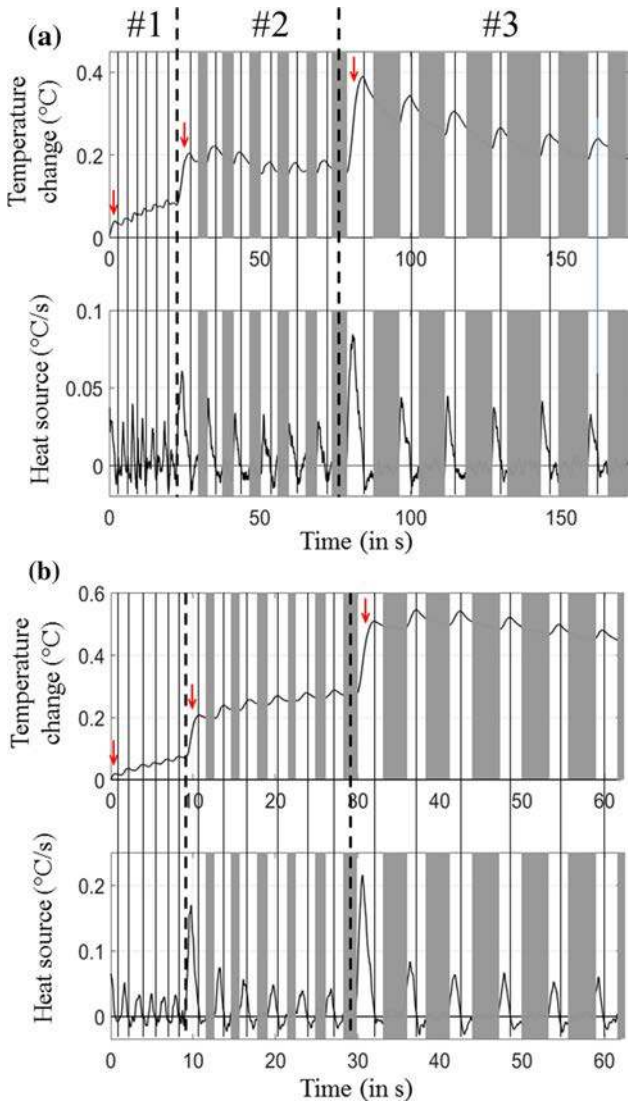

Figure 8 Cyclic tests for leather D. Gray zones correspond to specimen buckling. Vertical black lines correspond to the maximum stretch in each mechanical cycle. **a** Cyclic test at ± 100 mm/min. **b** Cyclic test at ± 300 mm/min.

rubber-like materials. Typically, it produced heat at the start of loading. Moreover, a strong similarity with the Mullins effect in rubber materials was observed in both the mechanical and the calorimetric responses;

- the presence of plasticizer in the tested leathers led to a higher level of heat production throughout the tests, probably due to the additional viscosity induced.

This type of information could be used to propose accurate thermomechanical behavior laws for specific leathers. An analysis of the tearing response of leathers is also available in [46], in which investigations were carried out at the local scale using two full-field techniques (IR thermography and digital image correlation) in order to discuss the material's resistance in terms of thermal activity in the crack zone of influence. Finally, temperature measurements under stretching may be used for quality control at different steps of the manufacturing process, in order, for instance, to assess viscosity properties from the material's calorific response.

Acknowledgements

The authors thank the National Center for Scientific Research (MRCT-CNRS and MI-CNRS), Rennes Metropole and Region Bretagne for financially supporting this work. Authors also thank Dr Mathieu Miroir, Dr Eric Robin, Mr Vincent Burgaud and Mr Mickaël Lefur for having designed the biaxial tensile machine, and Dr Pierre-Olivier Bussiere for the chemical analyses. The authors also thank the Campus des Métiers et des Qualifications "Design, Matériaux & Innovation" for supporting this work.

Compliance with ethical standards

Conflict of interests The authors declared no potential conflicts of interest with respect to the research, authorship and/or publication of this article.

References

[1] Ewans WD, Critchfield CL (1933) The effect of atmospheric moisture on the physical properties of vegetable and chrome tanned calf leathers. Bur Stand J Res 11:147–162

[2] Mitton RG (1945) Mechanical properties of leather fibres. J Int Soc Leather Trades' Chem 29:169–194

[3] Mitton RG (1948) Tensile properties and their variability in chrome-tanned calfskin. J Soc Leather Trades' Chem 32:310–323

[4] Lin J, Hayhurst DR, Howard IC, Reedman DC (1992) Modeling of the performance of leather in a uniaxial shoe-last simulator. J Strain Anal Eng Des 27:187–196

[5] Makho K (1998) The effect of different parameters on the rupture properties of leather in a tensile test. Master thesis dissertation, Faculty of science, Physics and Electronics, Rhodes University (South Africa)

[6] Wright DM, Attenburrow GE (2000) The set and mechanical behaviour of partially processed leather dried under strain. J Mater Sci 35:1353–1357. https://doi.org/10.1023/A:1004725922870

[7] Manich AM, de Castellar MD, Gonzalez B, Ussman MH, Marsal A (2006) Influence of leather stretching to gain area yield on its stress-relaxation behavior. J Appl Polym Sci 102:6000–6008

[8] Liu CK, Latona NP, DiMaio GL, Cooke PH (2007) Viscoelasticity studies for a fibrous collagen material: chrome-free leather. J Mater Sci 42:8509–8516. https://doi.org/10.1007/s10853-007-1744-1

[9] Bison PG, Grinzato E, Marinetti S (2005) Leather characterisation by IR thermography. In: Peacock GR, Burleigh DD, Miles JJ (eds) Proceedings of the society of the photo-optical instrumentation engineers (SPIE), vol 5782, pp 359–370

[10] Luong MP (1999) Evaluation of the limit of acceptable damage for leather products using infrared thermography. In: Baaklini GY, Lebowitz CA, Boltz ES (eds) Nondestructive evaluation of aging materials and composites III, Proc SPIE, vol 3585, pp 84–95

[11] Luong MP (1999) Evaluating a limit of acceptable damage for leather products. In: Ellyin F, Provan JW (eds) Progress in mechanical behavior of materials (ICM8), vol 2: materials properties. University of Victoria, Department of Mechanical Engineering, Canada, pp 523–528

[12] Luong MP (1999) Infrared thermography of damage evaluation in leather products. In: Melker AI (ed) Proceedings of the society of the photo-optical instrumentation engineers (SPIE), vol 3687, pp 191–200

[13] Chrysochoos A, Dupré JC (1991) Experimental analysis of thermomechanical coupling by infra-red thermography. In: Boehler JP, Khan JP (eds) Anisotropy and localization of plastic deformation. Springer, Dordrecht, pp 540–543

[14] Meyer KH, Ferri C (1935) Sur l'élasticité du caoutchouc. Helv Chim Acta 18:570–589

[15] Treloar LRG (1973) The elasticity and related properties of rubbers. Rep Prog Phys 36:755–826

[16] Chadwick P (1974) Thermo-mechanics of rubberlike materials. Philos T Roy Soc A 276:371–403

[17] Chrysochoos A (1995) Analyse du comportement des matériaux par thermographie infrarouge. In: Berthaud Y (ed) Photomécanique 95, Cachan, France, 14–16 March, 1995. Eyrolles (France), pp 203–211

[18] Chrysochoos A, Louche H (2000) An infrared image processing to analyse the calorific effects accompanying strain localization. Int J Eng Sci 38:1759–1788

[19] Samaca Martinez JR, Le Cam JB, Balandraud X, Toussaint E, Caillard J (2013) Mechanisms of deformation in crystallizable natural rubber. Part 1: thermal characterization. Polymer 54:2727–2736

[20] Samaca Martinez JR, Le Cam JB, Balandraud X, Toussaint E, Caillard J (2013) Filler effects on the thermomechanical response of stretched rubbers. Polym Test 32:835–841

[21] Samaca Martinez JR, Le Cam JB, Balandraud X, Toussaint E, Caillard J (2014) New elements concerning the Mullins effect: a thermomechanical analysis. Eur Polym J 55:98–107

[22] Balandraud X, Le Cam JB (2014) Some specific features and consequences of the thermal response of rubber under cyclic mechanical loading. Arch Appl Mech 84:773–788

[23] Le Cam JB, Samaca Martinez JR, Balandraud X, Toussaint E, Caillard J (2015) Thermomechanical analysis of the singular behavior of rubber: entropic elasticity, reinforcement by fillers, strain-induced crystallization and the Mullins effect. Exp Mech 55:771–782

[24] Le Cam JB (2017) Energy storage due to strain-induced crystallization in natural rubber: the physical origin of the mechanical hysteresis. Polymer 127:166–173

[25] Le Cam JB (2018) Strain-induced crystallization in rubber: a new measurement technique. Strain 54:e12256. https://doi.org/10.1111/str.12256

[26] Chrysochoos A, Pham H, Maisonneuve O (1996) Energy balance of thermoelastic martensite transformation under stress. Nucl Eng Des 162:1–12

[27] Balandraud X, Ernst E, Soos E (1999) Rheological phenomena in shape memory alloys. CR Acad Sci II B 327:33–39

[28] Balandraud X, Ernst E, Soos E (2000) Relaxation and creep phenomena in shape memory alloys. Part II: stress relaxation and strain creep during phase transformation. Z Angew Math Phys 51:419–448

[29] Balandraud X, Ernst E, Soos E (2000) Relaxation and creep phenomena in shape memory alloys. Part I: hysteresis loop and pseudoelastic behavior. Z Angew Math Phys 51:171–203

[30] Bubulinca C, Balandraud X, Grédiac M, Stanciu S, Abrudeanu M (2014) Characterization of the mechanical dissipation in shape-memory alloys during stress-induced phase transformation. J Mater Sci 49:701–709. https://doi.org/10.1007/s10853-013-7751-5

[31] Delobelle V, Favier D, Louche H, Connesson N (2015) Determination of local thermophysical properties and heat of transition from thermal fields measurement during drop calorimetric experiment. Exp Mech 55:711–723

[32] Delpueyo D, Balandraud X, Grédiac M, Stanciu S, Cimpoesu N (2018) A specific device for enhanced measurement of mechanical dissipation in specimens subjected to long-term tensile tests in fatigue. Strain 54:e12252. https://doi.org/10.1111/str.12252

[33] Benaarbia A, Chrysochoos A, Robert G (2014) Kinetics of stored and dissipated energies associated with cyclic loadings of dry polyamide 6.6 specimens. Polym Test 34:155–167

[34] Benaarbia A, Chrysochoos A, Robert G (2014) Influence of relative humidity and loading frequency on the PA6.6 cyclic thermomechanical behavior: part I. Mechanical and thermal aspects. Polym Test 40:290–298

[35] Benaarbia A, Chrysochoos A, Robert G (2015) Thermomechanical behavior of PA6.6 composites subjected to low cycle fatigue. Compos Part B-Eng 76:52–64

[36] Benaarbia A, Chrysochoos A, Robert G (2015) Influence of relative humidity and loading frequency on the PA6.6 thermomechanical cyclic behavior: part II. Energy aspects. Polym Test 41:92–98

[37] Benaarbia A, Chrysochoos A, Robert G (2015) Fiber orientation effects on heat source distribution in reinforced polyamide 6.6 subjected to low cycle fatigue. J Eng Math 90:13–36

[38] Jongchansitto P, Douellou C, Preechawuttipong I, Balandraud X (2018) Comparison between 0D and 1D approaches for mechanical dissipation measurement during fatigue tests. Strain (submitted)

[39] Giancane S, Chrysochoos A, Dattoma V, Wattrisse B (2009) Deformation and dissipated energies for high cycle fatigue of 2024-T3 aluminium alloy. Theor Appl Fract Mec 52:117–121

[40] Boulanger T, Chrysochoos A, Mabru C, Galtier A (2004) Calorimetric analysis of dissipative and thermoelastic effects associated with the fatigue behavior of steels. Int J Fatigue 26:221–229

[41] Wang XG, Crupi V, Jiang C, Feng ES, Guglielmino E, Wang CS (2017) Energy-based approach for fatigue life prediction of pure copper. Int J Fatigue 104:243–250

[42] ASTM D2209-00 (2015) Standard test method for tensile strength of leather. ASTM International, West Conshohocken

[43] ASTM D2211–00 (2015) Standard test method for elongation of leather. ASTM International, West Conshohocken, p 201542

[44] ASTM D412-16 (2016) Standard test methods for vulcanized rubber and thermoplastic elastomers-tension. ASTM International, West Conshohocken

[45] Mullins L (1948) Effect of stretching on the properties of rubber. Rubber Chem Technol 21:281–300

[46] Di Cesare N, Corvec G, Le Cam JB, Balandraud X, Gauffreteau J (2018) Tearing behavior of two types of leather: a comparative study carried out at the local scale using full kinematic and thermal field measurement techniques. Strain (submitted)